Correlation between Quasielastic Raman Scattering and Configurational Entropy in an Ionic Liquid†

Mauro C. C. Ribeiro*

Laboratório de Espectroscopia Molecular, Instituto de Química, Universidade de São Paulo, C.P. 26077, CEP 05513-970, São Paulo, SP, Brazil

Received: June 19, 2006; In Final Form: August 16, 2006

Low-frequency (5−200 cm^{-1}) Raman spectra are reported for the ionic liquid 1-butyl-3-methylimidazolium hexafluorophosphate, [bmim]PF_6, in glassy, supercooled liquid, and normal liquid phases (77−330 K). Raman spectra of [bmim]PF_6 agree with previous results obtained by optical Kerr effect spectroscopy and molecular dynamics simulation. Both the superposition model and the coupling model give reasonable fit to low-frequency Raman spectra of [bmim]PF_6. The configurational entropy of [bmim]PF_6 has been evaluated as a function of temperature using recently reported data of heat capacity. The calculated configurational entropy is inserted in the Adam−Gibbs theory for supercooled liquids, giving a good fit to non-Arrhenius behavior of viscosity and diffusive process, with the latter revealed by a recent neutron scattering investigation of [bmim]PF_6. There is a remarkable linear dependence between intensity of quasielastic Raman scattering and configurational entropy from 77 K up to the melting point of [bmim]PF_6. This correlation offers insight into the nature of dynamical processes probed by low-frequency Raman spectra of ionic liquids.

Introduction

Ionic liquid is a concise nomenclature that is now accepted for purely ionic systems with low melting point, e.g., below ∼100 °C, formerly called room-temperature molten salts.[1−3] A large diversity of ionic liquids has been synthesized by combining many different anions and cations, with the common characteristic of including large asymmetric organic ions that reduce the strong Coulombic interactions present in a molten salt and also preclude efficient crystal packing. The most investigated ionic liquids are based on imidazolium cations, in particular, derivatives of 1-alkyl-3-methylimidazolium cation (see Figure 1). The most important application of ionic liquids is alternative solvents in organic chemistry synthesis, followed by their use as media for eletrochemical applications, and extraction of both organic and inorganic species. Due to their technological interest, the demand is evident for fundamental physicochemical data on ionic liquids, such as density, viscosity, conductivity, and so forth.[1−3] On the other hand, understanding macroscopic properties on the basis of a microscopic picture of molecular structure and dynamics has led to a growing body of information on ionic liquids obtained from the combined usage of several spectroscopic techniques.[4−8] Experimental data have been complemented with theoretical investigations, either from quantum chemical calculations of an isolated ionic pair or cluster of ions[9−11] or from classical computer simulations of the condensed phase.[12−16]

Raman spectroscopy sheds light on important structural features of ionic liquids, such as anion−cation interactions,[17] hydrogen bonding,[18] solvation of probe molecules,[19] conformation of alkyl chains,[20] or ionic pair formation in solutions of lithium salts in ionic liquids.[21] In these (high-frequency) Raman studies of ionic liquids, assignment of vibrational (intramolecular) modes might be achieved with the help of quantum chemical calculations. On the other hand, Raman spectroscopy of glass-forming liquids has been the subject of many investigations in the past decades, in which attention is paid to the low wavenumber range of the Raman spectrum.[22−28] It is well-known that ionic liquids are good glass-formers, that is, several ionic liquids do not crystallize when cooled below the melting temperature, T_m, thus becoming a supercooled liquid, and reaching an amorphous solid state, i.e. the glassy state, upon further cooling below the glass transition temperature, T_g.[29,30] Low-frequency Raman spectra of supercooled liquids, typically in the $5 < \omega < 200$ cm^{-1} range, exhibit a rather universal pattern resulting from vibrational (intermolecular) dynamics plus relaxation processes. The fast relaxational motions, within a time range of picoseconds, appear as a quasielastic scattering (QES) peak, which can be modeled by a Lorentzian band at zero wavenumber within a few wavenumbers of bandwidth. The QES intensity decreases with falling temperature, as it is dependent on the dynamics of relaxation.

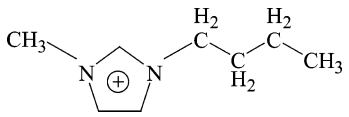

Figure 1. The structure of the 1-butyl-3-methylimidazolium cation, $[bmim]^+$.

To the author's knowledge, imidazolium ionic liquids have not been the subject of a low-frequency Raman study. In the low-frequency range, vibrational dynamics of ionic liquids have been revealed by time-resolved optical Kerr effect (OKE) spectroscopy.[31−35] Upon analysis of OKE spectra, the long relaxation time observed in the time-domain data is first removed by fitting a slowly decaying exponential function. This procedure gives a short-time (subpicosecond) oscillatory pattern in time, which by Fourier transforming provides the frequency spectra of intermolecular vibrations. This same frequency range is accessible by molecular dynamics (MD) simulations. In fact,

† Part of the special issue "Physical Chemistry of Ionic Liquids".

* E-mail: mccribei@iq.usp.br.

10.1021/jp063810r CCC: $37.00
Published on Web 09/30/2006

previous MD investigation of ionic liquids gave vibrational density of states very similar to OKE spectra.[36]

The first aim of this work is a low-frequency Raman investigation of the ionic liquid 1-butyl-3-methylimidazolium hexafluorophosphate, [bmim]PF_6, whose T_m and T_g are 283 and 191 K, respectively.[37] This particular system has been chosen because it is a representative example of ionic liquids containing imidazolium cations, so that basic physicochemical properties have been reported for [bmim]PF_6.[2,37−40] It has been the subject of many spectroscopic studies, such as NMR,[41,42] X-ray,[43] neutron scattering,[44,45] OKE,[32] and (high-frequency) Raman spectroscopy,[46] and theoretical studies by quantum chemical calculation[46,47] and MD simulation.[14,15,36,48−52] In this work, a comparison between low-frequency Raman spectra with previous OKE[32] and MD[36] data is performed, indicating the consistency between them. It will be shown that two usual approaches for modeling low-frequency Raman spectra of glass-forming liquids, the superposition model and the coupling model,[53−56] are also valid for [bmim]PF_6. In the superposition model, vibrational and relaxational processes are assumed to be independent of each other, so that the Raman spectrum is a simple sum of these two contributions. Conversely, in the coupling model, intermolecular vibrations are coupled with relaxation processes, and the Raman spectrum is a convolution of these contributions.[53] Both are phenomenological models that give a reasonable fit to experimental Raman spectra. The coupling model has been developed further, since the empirical parameter that measures the coupling between vibrational and relaxational modes, δ, has been related to free volume, V_f.[57,58] In free volume theories, transport coefficients increase on cooling the system due to exponential dependence of structural relaxation time with V_f.[29,30] Therefore, the correlation between V_f and δ links fast relaxation processes probed by QES with the slow structural α-relaxation time.

The second and far-reaching goal of this work is an interpretation of QES in [bmim]PF_6 on the basis of configurational entropy and not on the basis of free volume theories. The configurational entropy, S_c, plays a key role in the Adam−Gibbs theory for the temperature dependence of transport coefficients in supercooled liquids.[59] According to the Adam−Gibbs theory, assemblies of particles, the so-called cooperatively rearranging region, CRR, experience transitions between distinct configurations so that the probability of such transitions dictates the structural relaxation. The size of CRRs increases on cooling the system down to T_g, and the relaxation time depends exponentially on this size. The connection between a transport coefficient and thermodynamics is achieved, since the critical size of the CRR is inversely proportional to S_c. When testing the Adam−Gibbs theory, S_c is usually considered as the excess entropy, S_{exc}, which is directly evaluated by integrating the difference between the heat capacities of liquid and crystalline phases as a function of temperature.[60−66]

Fortunately, a detailed investigation of heat capacity, C_p, of [bmim]PF_6 has been recently reported, covering its normal liquid, supercooled liquid, glassy, and crystalline phases.[37] In this work, S_{exc} of [bmim]PF_6 will be calculated from these reported C_p data. On the other hand, S_c formally differs from experimental S_{exc} because the vibrational contribution to entropy of a supercooled liquid is not the same as in the crystalline phase.[67,68] It has been proposed that S_{exc} should be reduced by an appropriate accounting of vibrational contributions separately, giving a better estimate for the true S_c of a supercooled liquid.[67−69] In this work, it will be shown that a combination of experimental C_p [37] together with previously calculated C_p for a hypothetical ideal gas of [bmim]PF_6 [70] gives a more satisfactory description of S_c. In fact, it will be shown that the temperature behavior of viscosity, and also the relaxation time of diffusive processes reported in a recent neutron scattering investigation of [bmim]PF_6,[45] is captured by the Adam−Gibbs theory, provided that S_c, and not simply S_{exc}, is used in the theory.

The linear relationship between the QES signal intensity and S_c establishes a correlation between these two entities. The correlation between QES and S_c in [bmim]PF_6 covers an extended temperature range, from the glassy state at 77 K, through the whole range of supercooled liquid, up to the melting point. Furthermore, neutron scattering spectroscopy[45] has revealed a hierarchy of dynamical processes in [bmim]PF_6 that are gradually accessed when the temperature increases. A similar physical picture is proposed here on the basis of simultaneous increasing of QES signal and S_c upon heating the ionic liquid [bmim]PF_6 from the glassy, through the supercooled liquid, up to the normal liquid phase.

Experimental Section

The ionic liquid 1-butyl-3-methylimidazolium hexafluorophosphate, [bmim]PF_6, (Aldrich) was dried at 40 °C under high vacuum for ca. 48 h and sealed in a glass tube for spectroscopy measurements. Raman spectra were recorded with a Jobin-Yvon U-1000 double monochromator spectrometer equipped with a RCA C31034A phototube. Spectra were excited with the 647.1 nm line of a Coherent Innova 90 Kr^+ laser, typically with 300 mW of output power. Spectral resolution was kept at 2.0 cm^{-1}, and no modification of band shape was observed by changing resolution within the 1.0−3.0 cm^{-1} range. Raman spectra were recorded each 0.5 cm^{-1} from 5.0 to 500.0 cm^{-1}, in which intramolecular bands observed above 200.0 cm^{-1} were used to normalize the data at different temperatures. Temperature control was achieved with an Optistat cryostat of Oxford Instruments filled with liquid nitrogen, so that the lowest accessible temperature was 77 K. Low-temperature spectra were obtained by stepwise cooling from room temperature, resting ca. half an hour in a given temperature for equilibration, plus half an hour for data acquisition. Spectra at different temperatures shown below were obtained at different days, revealing that band shapes, and the relative weight of vibrational and relaxational contributions, were not dependent on slight changes in the thermal history of the sample. (It is worth mentioning that crystallization is observed at ca. 220 K upon heating glassy [bmim]PF_6.) Raman spectra were recorded in the usual 90° geometry, by using a polaroid to select polarized (I_{VV}) and depolarized (I_{VH}) components, and also with no polarization selection. In the 5−200 cm^{-1} range, similar band shapes were obtained for I_{VV}, I_{VH}, and the total spectra with no polarization selection. Of course, the latter gives higher signal-to-noise ratio, and it is presented in figures below.

Results and Discussion

Quasielastic Raman Scattering of [bmim]PF_6. Figure 2 shows representative low-frequency Raman spectra of [bmim]PF_6 in terms of reduced Raman spectra $I_{red}(\omega)$[23−28,53−58]

$$I_{red}(\omega) = \frac{I(\omega)}{\omega[\langle n(\omega)\rangle + 1]} \quad (1)$$

where $I(\omega)$ is the experimental spectrum in a given temperature T, and $\langle n(\omega)\rangle$ is the thermal population factor, $\langle n(\omega)\rangle = [\exp(h\omega/kT) - 1]^{-1}$. Both polarized and depolarized Raman spectra display very similar band shapes, implying constant depolar-

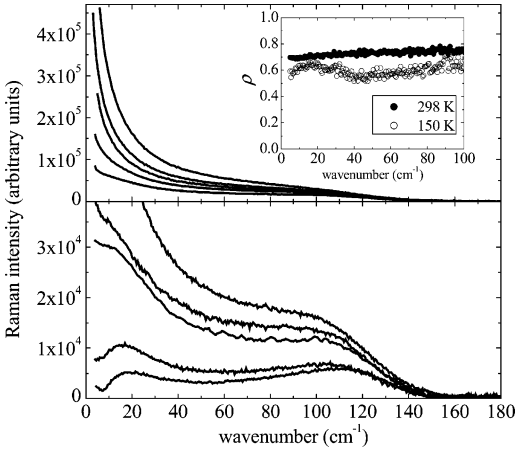

Figure 2. Low-frequency Raman spectra of [bmim]PF_6 with no polarization selection. From high to low intensity, the top panel shows spectra at 330, 298, 280, 240, and 210 K, and the bottom panel shows, in a different intensity scale, spectra at 210, 190, 170, 120, and 77 K. Experimental melting and glass transition of [bmim]PF_6 is reported at $T_m = 283$ K and $T_g = 191$ K.[37] Inset shows depolarization ratio at 298 K (black circles) and 150 K (white circles).

ization ratio, $\rho = I_{VH}/I_{VV}$, in the $5 < \omega < 100$ cm^{-1} range (see inset of Figure 2). In the low-frequency range, constant ρ has been observed close to the maximum value in several systems, such as LiCl aqueous solution,[23] $GeSBr_2$,[54] propylene glycol,[57] and other organic glass-forming liquids.[53] Smaller ρ has been observed in (high-temperature) molten salts.[26,27,71] In an attempt to explain small ρ in molten salts, Madden et al.[72] proposed that short-range and field contributions should be included in the fluctuation of polarizability, in addition to dipole−induced-dipole (DID) and reorientational mechanisms that give $\rho = 0.75$. In the case of the glass-forming system $2BiCl_3$−KCl, small ρ was explained on the basis of charge−current contributions.[73] This arises from the distinctive structural feature of a molten salt, i.e., charge ordering, which was also revealed in imidazolium ionic liquids by MD simulations.[12−16,36,48−52] Nevertheless, concerning the depolarization ratio of low-frequency Raman spectra, [bmim]PF_6 recalls the previous finding in organic glass-formers.

The quasielastic scattering (QES) intensity drops significantly when cooling [bmim]PF_6, so that intermolecular vibrational dynamics, giving at least two clear peaks at 20 and 110 cm^{-1}, is revealed at the lowest temperature. One sees in Figure 2 that, in comparison with the glass at 77 K, these low-frequency peaks shift to lower wavenumber when temperature increases. Overall, the way that low-frequency Raman spectra of [bmim]PF_6 change with decreasing temperature, displaying decreasing relaxational contribution from the normal liquid state down to the glassy state, is analogous to well-known features of Raman spectra already observed in many glass-formers.

The double-peaked pattern of the intermolecular vibrational dynamics, seen in the low temperature spectrum of Figure 2, promptly remind us of corresponding data obtained by optical Kerr effect (OKE) spectroscopy[32] and molecular dynamics (MD) simulation[36] of [bmim]PF_6 at high temperature. Figure 3 provides a comparison between Raman, OKE, and MD data for [bmim]PF_6. Bearing in mind the distinct nature of each data, the correlation between these results is noteworthy. The OKE result is only the vibrational (subpicosecond) dynamics, since long-time reorientational dynamics has been removed from the time domain data by fitting a slowly decaying exponential function. Very similar OKE spectra have been reported for other ionic liquids based on imidazolium cations with alkyl chains

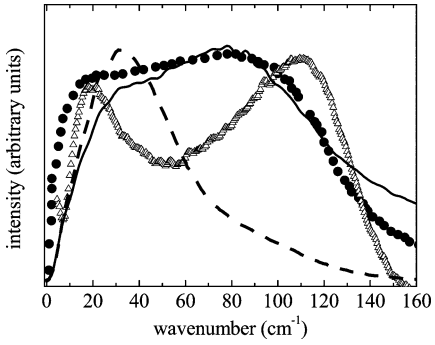

Figure 3. Comparison between Raman spectrum of [bmim]PF_6 at 77 K (white triangles), OKE spectrum at room temperature (black circles),[32] and vibrational density of states, DOS, calculated by MD simulation of [bmim]PF_6 at 400 K[36] (dashed line, partial anion DOS; full line, partial cation DOS).

of different length and also with different anions.[31,33,34] On the other hand, the MD result is the vibrational density of states (DOS) obtained by Fourier transforming the time autocorrelation function of particle velocities, $C(t) = \langle \mathbf{v}_i(t) \cdot \mathbf{v}_i(0) \rangle$, where $\mathbf{v}_i$ is the velocity of a given atom i. (Details about the protocol employed in the MD simulations can be found in refs 15 and 36.) It is clear from partial cation and anion DOS in Figure 3 that anions contribute to the band at lower wavenumber, whereas cations contribute to the broad band at higher wavenumber. It is worth mentioning that DOS differs from experimental spectrum, because the latter depends on the ability of a particular motion to modulate the polarizability of the material.[72,74−76] Such a dependence of polarizability on ionic displacement and reorientation is not being taken into account in calculated DOS. Thus, the finding that the vibrational motions revealed by low-temperature Raman spectra follows closely the calculated DOS strongly suggests that the light−vibration coupling in [bmim]PF_6 is almost frequency-independent in the low wavenumber range. It should be noted that results shown in Figure 3 correspond to different temperatures, so that disagreement in the exact peak positions is not unexpected. Raman and OKE spectra correspond to 77 and 298 K, respectively, and the MD result corresponds to a simulation performed in a relatively high temperature ($T = 400$ K) in order to achieve reasonable ionic mobility and satisfactory statistics. In fact, one finds a significant softening of the high-frequency band at ~100 cm^{-1} when [bmim]PF_6 is heated from glassy to liquid state (see Figure 2, and also Figure 4 below).

The superposition model assumes that $I_{red}(\omega)$ is the sum of a central peak, accounting for relaxational motions, plus a vibrational contribution at a finite wavenumber.[25,27,54−56,73] The relative weight of relaxational and vibrational contributions changes with temperature. In the case of [bmim]PF_6, we found a satisfactory fit of $I_{red}(\omega)$ in a given T by using the 77 K Raman spectrum as an approximation for the vibrational contribution, and a Lorentzian band at zero wavenumber for the relaxational contribution. The top panel of Figure 4 ilustrates the ability of the superposition model to fit the Raman spectrum of [bmim]PF_6 at room temperature. In the fit procedure, the 77 K spectrum had to be shifted by 20 cm^{-1} to a low wavenumber in order to match the high-frequency tail of the experimental spectrum at room temperature. This low-frequency shift of the 77 K spectrum accounts for the softening of intermolecular vibrations with increasing temperature.

In the coupling model, the calculation of $I_{red}(\omega)$ at any T follows by a convolution of vibrational and relaxational dynamics.[53,54,56−58] In this approach, one also needs the purely

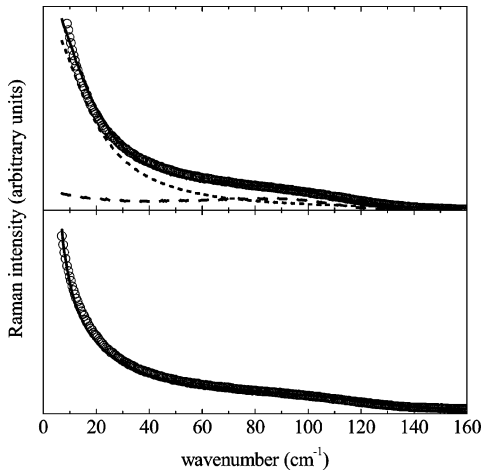

Figure 4. Best fit of Raman spectrum of [bmim]PF_6 at 298 K with the superposition model (top panel) and the coupling model (bottom panel). In each panel, white circles are experimental data, and full bold lines are calculated spectra. In the superposition model, the dotted line is the central Lorentzian component, and the dashed line is the experimental Raman spectrum at 77 K, which has been downshifted by 20 cm^{-1} and used as an approximation for the vibrational component. In the coupling model, the Raman spectrum at 77 K is also used as an approximation for $I_o(\omega)$ in eq 2, but no downshift is needed ($\delta = 75$ cm^{-1}, $\gamma = 150$ cm^{-1}).

vibrational spectrum, $I_o(\omega)$, which is usually estimated from the experimental Raman spectrum recorded in a very low temperature. According to the coupling model, $I_{red}(\omega)$ is given by

$$I_{red}(\omega) = \int \frac{I_o(\Omega)\Omega^2 \dfrac{\delta^2\gamma}{\omega^2+\gamma^2}}{\left(\Omega^2 - \omega^2 - \dfrac{\delta^2\gamma^2}{\omega^2+\gamma^2}\right)^2 + \left(\dfrac{\delta^2\gamma\omega}{\omega^2+\gamma^2}\right)^2} \mathrm{d}\Omega \quad (2)$$

where δ measures the strength of coupling between vibrational and relaxational motions, and γ measures the inverse of the relaxation time. The empirical parameter δ has been related to the fractional free volume V_f of supercooled liquids.[57,58] Novikov et al.[58] showed that previously measured V_f of polymeric glass-formers correlate with the estimative resulting from best fit δ. This finding links fast relaxation processes probed by QES with the structural α-relaxation time τ_α or a transport coefficient such as viscosity η, since free volume theories for supercooled liquids predict that τ_α or η are proportional to $\exp(1/V_f)$. To apply eq 2 to model Raman spectra of [bmim]PF_6, we used the 77 K spectrum as an approximation for $I_o(\omega)$. The bottom panel of Figure 4 shows that the coupling model also gives a satisfactory fit of $I_{red}(\omega)$ at room temperature. It is worth mentioning that, conversely to the superposition model, no low-frequency shift of the 77 K spectrum is needed when applying the coupling model.

In summary, Figure 4 indicates that the correctness of either the superposition or the coupling model is not resolved simply from the quality of fit to experimental data. Thus, in the following, we seek an interpretation of QES in [bmim]PF_6 that is not too dependent on an assumed model for the calculation of the Raman spectrum. In fact, it will be shown that configurational entropy of [bmim]PF_6 correlates with the intensity of the QES signal. The intensity of QES in a given temperature will be defined as the integral of the Raman spectrum up to 200 cm^{-1}, relative to the intensity of the 77 K spectrum. The temperature dependence of the QES intensity of [bmim]PF_6 is shown in Figure 5, in which glass transition and

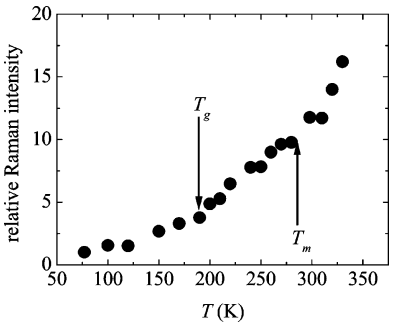

Figure 5. Integral of low-frequency Raman spectra of [bmim]PF_6 in the $5 < \omega < 200$ cm^{-1} range, normalized by the integral of the spectrum at 77 K.

melting temperatures are indicated by arrows. Distinct slopes can be noted at glassy, supercooled liquid, and normal liquid ranges, but one does not observe any discontinuity on QES intensity either at T_g or at T_m. The QES intensity grows about 10 times from deep-cooled glassy state at 77 K up to the melting temperature. The rate of increasing of QES intensity with temperature follows the increase of configurational entropy of [bmim]PF_6, as we will now discuss.

Configurational Entropy of [bmim]PF_6. Glass-forming liquids are classified as strong or fragile according to the temperature dependence of viscosity η.[77−79] In strong liquids, with the archetypic one being SiO_2, a linear dependence is observed in an Arrhenius plot $\ln(\eta) \times T^{-1}$. On the other hand, in fragile liquids, one finds bent $\ln(\eta) \times T^{-1}$ curves when T approaches T_g. In the temperature range covering the supercooled liquid state, $\eta(T)$ of fragile liquids is usually fit with the Vogel−Fulcher−Tammann (VFT) equation

$$\eta(T) \propto \exp\left(\frac{B}{T - T_o}\right) \quad (3)$$

with empirical B and T_o parameters. Organic liquids or molten salts with no directional intermolecular forces, for instance, $0.4Ca(NO_3)_2 \cdot 0.6KNO_3$, are typical fragile glass-forming liquids. It has been found that ionic liquids should be considered moderately fragile liquids.[80] Viscosity of ionic liquids has been also fit with the VFT equation, although reported data usually correspond to the normal liquid state above T_m. This is a rather small temperature range, and different authors reported a distinct set of best fit parameters when applying the VFT expression to the experimental data of [bmim]PF_6. For instance, within the $263 < T < 353$ K range, Tokuda et al.[40] found $B = 639$ K and $T_o = 201$ K, with the latter not being a very realistic parameter, because $T_o > T_g$ would imply diverging η even above the glass transition at $T_g = 191$ K. A more physically meaningful set of parameters for [bmim]PF_6 was obtained by Harris et al.,[39] $B = 1127$ K and $T_o = 161.8$ K. Other authors did not attempt a VFT fit of high-temperature $\eta(T)$, and polynomial functions were used to represent experimental data of [bmim]PF_6.[81,82]

In comparison with a strict Arrhenius dependence, the VFT equation suggests that the activation energy is no longer constant but is instead temperature-dependent. The Adam−Gibbs (AG) theory[59] allows for the calculation of the structural α-relaxation time τ_α, or a transport coefficient such as η, on the basis of thermodynamics considerations. The key concept in the AG theory is a cooperatively rearranging region (CRR) whose size $z(T)$ increases with decreasing temperature. The size $z(T)$ measures the number of particles participating in a region that is able to change its configuration without changing configuration in the neighborhoods, so that its asymptotic limits would

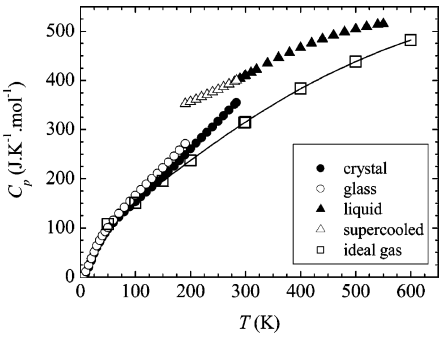

Figure 6. Heat capacity of [bmim]PF_6 in the crystalline (black circles), glassy (white circles), normal liquid (black triangles), and supercooled liquid (white triangles) phases as reported in ref 37. White squares give C_p of an ideal gas of [bmim]$^+ - PF_6^-$ ionic pairs evaluated by ab initio calculations,[70] and the full line is a polynomial interpolation through the data actually provided in ref 70.

be a single molecule at high temperature and the whole sample at very low temperature. The size $z(T)$ is inversely proportional to the configurational entropy S_c, from which one obtains an expression to compare calculated viscosity η^{AG} against experimental data

$$\eta^{AG}(T) \propto \exp\left(\frac{1}{TS_c}\right) \tag{4}$$

For eq 4 be useful, one needs the nontrivial temperature-dependent property S_c. In most cases, S_c is simply replaced by the excess entropy S_{exc}, which is evaluated by using experimental heat capacity C_p of liquid and crystalline phases[60−66]

$$S_{exc}(T) = \Delta S_{fus} - \int_{T'}^{T_{fus}} \frac{C_p^{l}(T') - C_p^{cr}(T')}{T'}\,dT' \tag{5}$$

where ΔS_{fus} is the entropy of fusion, and C_p^{cr} and C_p^{l} stand for heat capacity of crystalline and supercooled liquid phases, respectively. If one considers the entropy of the amorphous phase as a sum of configurational and vibrational contributions, $S_c + S_{vib}$, the replacement of S_c by S_{exc} assumes that S_{vib} is the same as the entropy of crystalline phase, an identity that is not strictly correct. It has been proposed that the vibrational contribution should be discounted from S_{exc} in order to result in a better estimative of S_c.[67−69,83] Yamamuro et al.[69] calculated vibrational C_p of some organic glass-formers, in which lattice vibrations and librations were approximated by Debye and Einstein functions, respectively, and intramolecular vibrations were considered on the basis of the experimental frequencies observed in infrared and Raman spectra.

Recently, a detailed investigation of C_p has been reported for glassy, supercooled liquid, normal liquid, and crystalline phases of [bmim]PF_6.[37] This study has been preceded by the calculation of C_p for an ideal gas of [bmim]PF_6.[70] In the calculation of C_p for ideal gas, the optimized structure of an ionic pair [bmim]$^+$−PF_6^- had been considered, plus intramolecular vibrations of each ion, obtained with ab initio quantum chemical calculations. The estimate of vibrational C_p in ref 70 accounted for inter- and intramolecular vibrations within a full ab initio calculation, in contrast to ref 69 where this task was achieved with the help of experimental vibrational frequencies. For completeness, Figure 6 shows experimental C_p for [bmim]PF_6 provided in Table 4 of ref 37. Calculated C_p of [bmim]$^+$−PF_6^- ionic pairs were provided at some selected temperatures in Table 8 of ref 70, and they are also shown in Figure 6 as white squares.

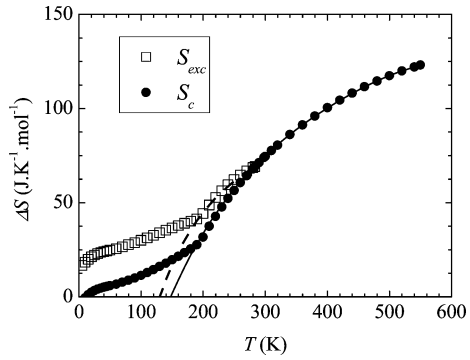

Figure 7. Calculated excess entropy (white squares) and configurational entropy (black circles) of [bmim]PF_6. The temperature range of S_{exc} is only below T_m. Dashed and full lines are polynomial fit to S_{exc} and S_c, respectively, through liquid-phase ranges.

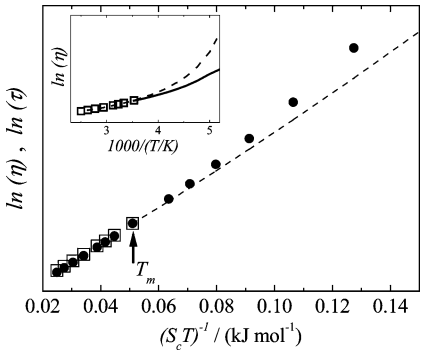

Figure 8. Adam−Gibbs plots for [bmim]PF_6. Black circles: relaxation time of diffusive processes revealed by neutron scattering spectroscopy.[45] White squares: viscosity in the normal liquid range,[39] where the dashed line is the extrapolation of η within the supercooled liquid range according to the VFT equation with best fit parameters provided in ref 39. Inset shows, in an Arrhenius plot, the same viscosity data of the main figure (white squares and dashes line), and resulting $(S_{exc}T)^{-1}$ in the supercooled liquid range (full line), i.e., using the excess entropy in the AG theory.

In this work, we use the experimental C_p data of ref 37 to evaluate S_{exc} according to eq 5 for $T < T_m$, where C_p^{l} stands for glassy state for $T < T_g$. Resulting S_{exc} is shown as white squares in Figure 7. The temperature dependence of S_{exc} resembles previous findings in several glass-formers, as it decreases sharply within the supercooled liquid range until T_g is reached, followed by a smaller slope within the glassy range. It should be noted that entropy is still being lost below T_g, including a further regime for T below ∼50 K. In a recent neutron scattering investigation of [bmim]PF_6 from the glassy state at 10 K up to the normal liquid state,[45] it has been observed that sequential dynamical processes are activated upon heating the system. Motions associated to the methyl group start at ∼80 K, then conformational changes of the butyl chain begin at ∼220 K, and finally diffusive processes at high temperature. This sequence of dynamical events observed by neutron scattering spectroscopy is consistent with the distinct regimes observed in S_{exc} as T increases.

The S_{exc} shown in Figure 7 was evaluated for glassy and supercooled liquid ranges of [bmim]PF_6, whereas experimental values of η are available for the normal liquid state above T_m.[39,40,81,82] Nevertheless, we found a clear misfit between experiment and the AG theory prediction for η when S_{exc} is used in eq 4. This is illustrated in the inset of Figure 8, where the dashed line is the extrapolation of the empirical VFT equation (eq 3) onto the supercooled liquid regime of [bmim]PF_6. To extend the AG calculation into the normal liquid range, in which

experimental η is available, it would be necessary to extrapolate C_p of crystalline phase shown in Figure 6 to high temperature. However, we found that high-temperature extrapolation of crystal C_p did not provide a reasonable agreement between experiment and theory, as already suggested in the inset of Figure 8.

We improved the AG prediction of the temperature dependence of transport coefficients in [bmim]PF_6 by using in eq 5 the vibrational C_p calculated in ref 70 as the vibrational contribution, instead of the experimental C_p of the crystalline phase. Figure 6 shows that C_p values for the ideal gas of $[bmim]^+-PF_6^-$ ionic pairs match C_p of the crystal at low temperatures, and above $T \approx 100$ K, it departs from the crystalline phase C_p. Ideal gas C_p values were not provided in ref 70 for temperatures below 50 K, so that we propose to merge the crystal-phase C_p data up to 100 K with the ideal gas C_p above 100 K as an estimate of purely vibrational contributions. (Results are not significantly affected by slight changes on the actual temperature below which the crystal phase C_p is used.) Since ideal gas C_p values were provided for high temperature,[70] by combining in eq 5 C_p data for crystalline (below 100 K) and ideal gas (above 100 K) phases, we calculated the entropy difference in the whole temperature range including glassy, supercooled liquid, and normal liquid phases, with the latter being the range in which experimental η is available. The resulting approximation for S_c is shown as black circles in Figure 7. There is a remarkable difference between S_{exc} and S_c in Figure 7: whereas residual S_{exc} remains, S_c in fact reaches zero at $T \rightarrow 0$. This finding suggests that the proposed consideration of vibrational C_p gives a reasonable estimative of S_c of [bmim]PF_6.

It is clear from Figure 7 that S_{exc} and S_c present slightly different slopes in the supercooled liquid range. In fact, by using a polynomial fit to entropy data above T_g, and then extrapolating to zero, different Kauzmann temperatures T_K [84] are found from S_{exc} or S_c. From S_{exc}, one obtains $T_K = 130$ K, whereas from S_c, one obtains $T_K = 150$ K, which is in closer agreement with $T_o = 161.8$ K reported in ref 39 on the basis of fitting the VFT equation to high-temperature viscosity data. However, it remains to be shown whether the calculated S_c results in a satisfactory fit to experimental data of [bmim]PF_6 when used in the AG expression (eq 4). Figure 8 shows Adam−Gibbs plots of experimental η[39] and the relaxation time τ of diffusive processes probed by neutron scattering spectroscopy.[45] The temperature range in which η of [bmim]PF_6 was measured cover the normal liquid phase, $273 < T < 353$ K (white squares),[39] so that the dashed line is the extrapolation of η within the supercooled liquid range by the VFT equation provided in ref 39. The black circles in Figure 8 are the behavior of $\tau(T)$, whose temperature dependence was also reproduced with a VFT expression.[45] It is clear from the linear dependence of Figure 8 that the AG theory gives a satisfactory prediction for both $\eta(T)$ and $\tau(T)$, provided that S_c (black circles in Figure 7) be used in eq 4. The agreement between AG theory and experiment extends for a rather large temperature range in the case of [bmim]PF_6. This finding resembles previous conclusions obtained for 3-bromopentane,[64] whereas a more limited temperature range of agreement between theory and experiment has been found in other organic glass-formers.[65]

In summary, the temperature dependence of viscosity and relaxation time of [bmim]PF_6 are well-described by the AG theory, as long as one does not use simply S_{exc} as the configurational entropy. The way that C_p data of [bmim]PF_6 have been decomposed here, namely, by considering purely vibrational contributions, has been already suggested in the calculation of S_c of organic glass-formers.[69] It seems that such an approach also works in the case of [bmim]PF_6, as indicated by the appropriateness of the AG theory to reproduce experimental transport coefficients (Figure 8). This finding corroborates the accuracy of ab initio calculations of structure and vibrational frequencies of the ionic pair $[bmim]^+-PF_6^-$ performed in ref 70. Furthermore, since the AG theory provides an important connection between transport coefficients and thermodynamic properties, the evaluation of S_c with the help of ab initio calculations for estimating vibrational contributions to C_p adds a further piece of information that connects structure, dynamics, and thermodynamics of ionic liquids.

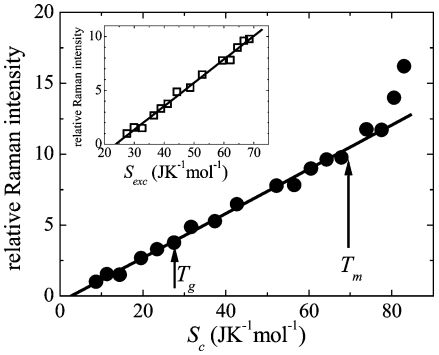

Figure 9. Correlation between the intensity of quasielastic scattering (Figure 5) and S_c (Figure 7) for [bmim]PF_6. Full line is a linear fit within the $77 < T < 310$ K range. Inset shows the corresponding correlation between QES and S_{exc} (white squares in Figure 7) within the glassy and supercooled liquid range.

Correlation between QES and S_c. The rates that both QES signal and S_c increase with temperature (Figures 5 and 7, respectively) are very similar. In fact, Figure 9 shows a nice linear relationship between these two sets of data, covering an extended temperature range from the glass at 77 K, through the whole supercooled liquid range, up to the normal liquid just above T_m. The inset in Figure 9 shows the analogous linear relation between QES and S_{exc}, where the latter is obtained for $T < T_m$ (white squares in Figure 7). The correlation shown in Figure 9 is remarkable, as it connects experimental data of very distinct nature, and in the particular case of QES intensity vs S_{exc}, no model assumption is needed since it is a direct correlation between crude spectroscopic and calorimetric data. In addition, correlation between QES and S_c suggests that both types of data are probing the same dynamical events. A previous neutron scattering investigation of [bmim]PF_6 showed that distinct dynamic processes are sequentially triggered as the temperature increases.[45] It has been found that relaxation of alkyl groups starts already at temperatures below 100 K, followed by diffusive processes at high temperatures. The comparison shown in Figure 3 between Raman and OKE spectra and MD simulations also indicates short-time (rattling) dynamics of anions and cations occurring at low temperature, with vibrations and relaxation processes being coupled together according to the coupling model (see Figure 4).

It should be noted that the wavenumber range of QES corresponds to fast (picosecond) relaxation, so that its correlation with S_c should imply a consistent interpretation of the latter. In the AG theory, a relation is made between transport coefficients, or structural relaxation time, and the critical size z^* of the CRR[59]

$$\eta^{AG}(T) \propto \exp\left(\frac{z^*\Delta\mu}{RT}\right) \qquad (6)$$

where $\Delta\mu$ is the energy barrier for rearrangement. The previous

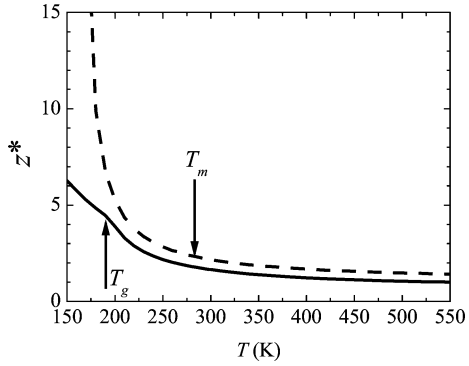

Figure 10. Critical size of cooperatively rearranging region evaluated from S_c of [bmim]PF_6 (full line). Dashed line is the $T/(T - T_o)$ result, with $T_o = 161.8$ K predicted from viscosity data.[39]

eq 4 follows by noting that $z^* = N_a s_c^*/S_c$, where s_c^* is the corresponding critical configurational entropy, N_a is the Avogadro number, and both $\Delta\mu$ and s_c^* are temperature-independent. Usually, one equates the empirical VFT expression, eq 3, with eq 6, obtaining $z^*(T)$ that increases from unity at $T \rightarrow \infty$ and diverges at T_o. If one considers diverging z^* at T_o, it is puzzling that the QES signal, which probes fast-dynamics relaxations, correlates with S_c through the whole range of supercooled [bmim]PF_6, including within the glassy state. Conversely, $z^*(T)$ can be estimated as the inverse of S_c, with the proviso of $z^* \rightarrow 1$ when $T \rightarrow \infty$. As is shown in Figure 10, a CRR would include less than 10 particles at T_g.[64,69,85]

MD simulations of simple models for glass-formers suggest that particles undergo local displacements within a given CRR, with structural relaxation being the result of rare fluctuations in CRRs.[86] It is now accepted that supercooled liquids develop dynamical heterogeneities, where a group of particles can be identified with mobility above the average.[87−89] MD simulation has been instrumental in revealing that such mobile particles might acquire stringlike structures of, for example, 10 particles in simple atomic Lennard-Jones models, and also in polymeric models in which the monomers follow each other in one-dimensional paths.[90] MD simulations also indicated a connection between spatially heterogeneous dynamics in supercooled liquids and the CRR.[91] It has been proposed that this relatively small group of mobile particles might be a candidate structure for the CRRs of the AG theory. Besides simple atomic models,[91] the relation between a cluster of mobile molecules and the CRRs has also been suggested by MD simulations of water[92] and *o*-terphenyl.[93] Thus, within a more localized physical picture for the CRRs, one conciliates that fast dynamical processes probed by QES follow the rate in which configurational entropy increases with temperature in the ionic liquid [bmim]PF_6.

Conclusions

In a previous publication,[36] it was shown that vibrational DOS obtained by MD simulations of ionic liquids are consistent with OKE spectra,[32] and this work added a third piece of experimental evidence, namely, low-frequency Raman spectra. The similarity between calculated DOS and vibrational dynamics revealed by Raman spectra of [bmim]PF_6 at low temperature suggests that the whole DOS is being probed, i.e., the light−vibration coupling is constant in the low-frequency range, so that Raman spectra reproduce the DOS. Usual models that have been used for the interpretation of Raman spectra of glass-formers, that is, the superposition model and the coupling model, also apply for the ionic liquid [bmim]PF_6. The superposition model became more precise when the adjustable parameter that measures the coupling between relaxational and vibrational motions was related with free volume.[57,58] In this work, instead of pursuing an interpretation of QES in terms of free volume theories, we pursued the route of the competing AG theory for the glass transition. Thus, it was first necessary to show that the AG theory gives a satisfactory description of the temperature dependence of transport coefficients of the ionic liquid [bmim]PF_6. Agreement between experiment and theory was not achieved when the excess entropy of [bmim]PF_6 was used in the AG expression. The configurational entropy was estimated instead by combining experimental C_p data[37] with calculated C_p of an ideal gas of $[bmim]^+-PF_6^-$ ionic pairs.[70] The correlation between these two types of experimental data, i.e., QES and S_c, was shown. The linear relation between QES and S_c indicates that both types of data are probing similar dynamical processes. On the basis of neutron scattering measurements on [bmim]PF_6,[45] it has been proposed that a sequence of dynamical processes is triggered as the system is heated from the deep glassy state up to the normal liquid state. The intensity of the QES signal and S_c of [bmim]PF_6 increase with temperature in such a way that suggests a correlation with the neutron scattering investigation of ref 45. Proper to the fast dynamics that low-frequency Raman spectra are able to probe, the CRRs proposed in the AG theory seems to conform with dynamical heterogeneity regions, as recently proposed on the basis of computer simulations of model liquids.[91−93] It would be interesting to determine whether the linear relation between QES intensity and S_c observed here for the ionic liquid [bmim]PF_6 also holds for other well-known organic glass formers. In the case of ionic liquids, to the author's knowledge, there is no similar detailed investigation of heat capacity for other imidazolium ionic liquids as reported in ref 37 for [bmim]PF_6. Nevertheless, ionic liquids with alkyl chains of different lengths deserve future low-frequency Raman investigations.

Acknowledgment. The author is indebted to FAPESP and CNPq for financial support.

References and Notes

(1) Welton, T. *Chem. Rev.* **1999**, *99*, 2071.
(2) Wasserscheid, P.; Welton, T. *Ionic Liquids in Synthesis*; Wiley: Weinheim, 2003.
(3) Buzzeo, M. C.; Evans, R. G.; Compton, R. G. *ChemPhysChem* **2004**, *8*, 1106.
(4) Hardacre, C.; Holbrey, J. D.; McMath, S. E. J.; Bowron, D. T.; Soper, A. K. *J. Chem. Phys.* **2003**, *118*, 273.
(5) Iimori, T.; Iwahashi, T.; Ishii, H.; Seki, K.; Ouchi, Y.; Ozawa, R.; Hamaguchi, H.; Kim, D. *Chem. Phys. Lett.* **2004**, *389*, 321.
(6) Hayamizu, K.; Aihara, Y.; Nakagawa, H.; Nukuda, T.; Price, W. S. *J. Phys. Chem. B* **2004**, *108*, 19527.
(7) Sloutskin, E.; Ocko, B. M.; Tamam, L.; Kuzmenko, I.; Gog, T.; Deutsch, M. *J. Am. Chem. Soc.* **2005**, *127*, 7796.
(8) Tokuda, H.; Ishii, K.; Susan, M. A. B. H.; Tsuzuki, S.; Hayamizu, K.; Watanabe, M. *J. Phys. Chem. B* **2006**, *110*, 2833.
(9) Turner, E. A.; Pye, C. C.; Singer, R. D. *J. Phys. Chem. A* **2003**, *107*, 2277.
(10) Liu, Z. P.; Huang, S. P.; Wang, W. C. *J. Phys. Chem. B* **2004**, *108*, 12978.
(11) Kossmann, S.; Thar, J.; Kirchner, B.; Hunt, P. A.; Welton, T. *J. Chem. Phys.* **2006**, *124*, 174506.
(12) Cadena, C.; Zhao, Q.; Snurr, R. Q.; Maginn, E. J. *J. Phys. Chem. B* **2006**, *110*, 2821.
(13) Wang, Y. T.; Izvekov, S.; Yan, T. Y.; Voth, G. A. *J. Phys. Chem. B* **2006**, *110*, 3564.
(14) Lynden-Bell, R. M.; Del Popolo, M. *Phys. Chem. Chem. Phys.* **2006**, *8*, 949.
(15) Urahata, S. M.; Ribeiro, M. C. C. *J. Chem. Phys.* **2004**, *120*, 1855; **2006**, *124*, 074513.
(16) Hunt, P. A. *Mol. Simul.* **2006**, *32*, 1.
(17) Heimer, N. E.; Del Sesto, R. E.; Meng, Z. Z.; Wilkes, J. S.; Carper, W. R. *J. Mol. Liq.* **2006**, *124*, 84.

(18) Chang, H. C.; Jiang, J. C.; Tsai, W. C.; Chen, G. C.; Lin, S. H. *J. Phys. Chem. B* **2006**, *110*, 3302.
(19) Fujisawa, T.; Fukuda, M.; Terazima, M.; Kimura, Y. *J. Phys. Chem. A* **2006**, *110*, 6164.
(20) Umebayashi, Y.; Fujimori, T.; Sukizaki, T.; Asada, M.; Fujii, K.; Kanzaki, R.; Ishiguro, S. *J. Phys. Chem. A* **2005**, *109*, 8976.
(21) Castriota, M.; Caruso, T.; Agostino, R. G.; Cazzanelli, E.; Henderson, W. A.; Passerini, S. *J. Phys. Chem. A* **2005**, *109*, 92.
(22) Winterling, G. *Phys. Rev.* **1975**, *12*, 2432.
(23) Tao, N. J.; Li, G.; Chen, X.; Du, W. M.; Cummins, H. Z. *Phys. Rev. A* **1991**, *44*, 6665.
(24) Krakoviack, V.; Alba-Simionesco, C.; Krauzman, M. *J. Chem. Phys.* **1997**, *107*, 3417.
(25) Kirillov, S. A.; Perova, T. S.; Nielsen, O. F.; Praestgaard, E.; Rasmussen, U.; Kolomiyets, T. M.; Voyiatzis, G. A.; Anastasiadis, S. H. *J. Mol. Struct.* **1999**, *479*, 271.
(26) Yannopoulos, S. N.; Papatheodorou, G. N. *Phys. Rev. B* **2000**, *62*, 3728.
(27) Yannopoulos, S. N.; Kastrissios, D. Th. *Phys. Rev. E* **2003**, *65*, 021510.
(28) Surovtsev, N. V.; Pugachev, A. M.; Nenashev, B. G.; Malinovsky, V. K. *J. Phys.: Condens. Matter* **2003**, *15*, 7651.
(29) Elliot, S. R. *Physics of Amorphous Materials*; Longman: Harlow, 1980.
(30) Varshneya, A. K. *Fundamentals of Inorganic Glasses*; Academic: New York, 1994.
(31) Hyun, B.-R.; Dzyuba, S. V.; Bartsch, R. A.; Quitevis, E. L. *J. Phys. Chem. A* **2002**, *106*, 7579.
(32) Giraud, G.; Gordon, C. M.; Dunkin, I. R.; Wynne, K. *J. Chem. Phys.* **2003**, *119*, 464.
(33) Cang, H.; Li, J.; Fayer, M. D. *J. Chem. Phys.* **2003**, *119*, 13017.
(34) Rajian, J. R.; Li, S.; Bartsch, R. A.; Quitevis, E. L. *Chem. Phys. Lett.* **2004**, *393*, 372.
(35) Shirota, H.; Funston, A. M.; Wishart, J. F.; Castner, E. W., Jr. *J. Chem. Phys.* **2003**, *122*, 184512.
(36) Urahata, S. M.; Ribeiro, M. C. C. *J. Chem. Phys.* **2005**, *122*, 024511.
(37) Kabo, G. J.; Blokhin, A. V.; Paulechka, Y. U.; Kabo, A. G.; Shymanovich, M. P.; Magee, J. W. *J. Chem. Eng. Data* **2004**, *49*, 453.
(38) de Azevedo, R. G.; Esperanca, J. M. S. S.; Najdanovic-Visak, V.; Visak, Z. P.; Guedes, H. J. R.; da Ponte, M. N.; Rebelo, L. P. N. *J. Chem. Eng. Data* **2005**, *50*, 997.
(39) Harris, K. R.; Woolf, L. A.; Kanakubo, M. *J. Chem. Eng. Data* **2005**, *50*, 1777.
(40) Tokuda, H.; Hayamizu, K.; Ishii, K.; Susan, Md. A. B. H.; Watanabe, M. *J. Phys. Chem. B* **2004**, *108*, 16593.
(41) Umecky, T.; Kanakubo, M.; Ikushima, Y. *Fluid Phase Equilib.* **2005**, *228*, 329.
(42) Antony, J. H.; Mertens, D.; Dolle, A.; Wasserchеid, P.; Carper, W. R. *ChemPhysChem* **2003**, *4*, 588.
(43) Hamaguchi, H.; Saha, S.; Ozawa, R.; Hayashi, S. *ACS Symp. Ser.* **2005**, *901*, 68.
(44) Triolo, A.; Russina, O.; Arrighi, V.; Juranyi, F.; Janssen, S.; Gordon, C. M. *J. Chem. Phys.* **2003**, *119*, 8549.
(45) Triolo, A.; Russina, O.; Hardacre, C.; Nieuwenhuyzen, M.; Gonzalez, M. A.; Grimm, H. *J. Phys. Chem. B* **2005**, *109*, 22061.
(46) Talaty, E. R.; Raja, S.; Storhaug, V. J.; Dolle, A.; Carper, W. R. *J. Phys. Chem. B* **2004**, *108*, 13177.
(47) Meng, Z.; Dolle, A.; Carper, W. R. *THEOCHEM* **2002**, *585*, 119.
(48) Margulis, C. J.; Stern, H. A.; Berne, B. J. *J. Phys. Chem. B* **2002**, *106*, 12017.
(49) Morrow, T. I.; Maggin, E. J. *J. Phys. Chem. B* **2002**, *106*, 12807.
(50) Znamensky, V.; Kobrak, M. N. *J. Phys. Chem. B* **2004**, *108*, 1072.
(51) Liu, Z.; Huang, S.; Wang, W. *J. Phys. Chem. B* **2004**, *108*, 12978.
(52) Lee, S. U.; Jung, J.; Han, Y. K. *Chem. Phys. Lett.* **2005**, *406*, 332.
(53) Gochiyaev, V. Z.; Malinovsky, V. K.; Novikov, Y. N.; Sokolov, A. P. *Philos. Mag. B* **1991**, *63*, 777.
(54) Krüger, M.; Soltwisch, M.; Petscherizin, I.; Quitmann, D. *J. Chem. Phys.* **1992**, *96*, 7352.
(55) Sokolov, A. P.; Kisliuh, A.; Quitmann, D.; Kudlik, A.; Rössler, E. *J. Non-Cryst. Solids* **1994**, *172−174*, 138.
(56) Terki, F.; Levelut, C.; Prat, J. L.; Boissier, M.; Pelous, J. *J. Phys.: Condens. Matter* **1997**, *9*, 3955.
(57) Kojima, S.; Novikov, V. N. *Phys. Rev. B* **1996**, *54*, 222.
(58) Novikov, V. N.; Sokolov, A. P.; Strube, B.; Surovtsev, N. V.; Duval, E.; Mermet, A. *J. Chem. Phys.* **1997**, *107*, 1057.
(59) Adam, G.; Gibbs, J. H. *J. Chem. Phys.* **1965**, *43*, 139.
(60) Greet, R. J.; Turnbull, D. *J. Chem. Phys.* **1967**, *47*, 2185.
(61) Magill, J. H. *J. Chem. Phys.* **1967**, *47*, 2802.
(62) Chang, S. S.; Bestul, A. B. *J. Chem. Phys.* **1972**, *56*, 503.
(63) Takeda, K.; Yamamuro, O.; Suga, H. *J. Phys. Chem.* **1995**, *99*, 1602.
(64) Takahara, S.; Yamamuro, O.; Matsuo, T. *J. Phys. Chem.* **1995**, *99*, 9589.
(65) Richert, R.; Angell, C. A. *J. Chem. Phys.* **1998**, *108*, 9016.
(66) Takeda, K.; Yamamuro, O.; Tsukushi, I.; Matsuo, T.; Suga, H. *J. Mol. Struct.* **1999**, *479*, 227.
(67) Johari, G. P. *J. Chem. Phys.* **2000**, *112*, 7518.
(68) Johari, G. P. *J. Chem. Phys.* **2000**, *112*, 8958.
(69) Yamamuro, O.; Tsukushi, I.; Lindqvist, A.; Takahara, S.; Ishikawa, M.; Matsuo, T. *J. Phys. Chem. B* **1998**, *102*, 1605.
(70) Paulechka, Y. U.; Kabo, G. J.; Blokhin, A. V.; Vydrov, O. A.; Magee, J. W.; Frenkel, M. *J. Chem. Eng. Data* **2003**, *48*, 457.
(71) McGreevy, R. K. *Solid State Phys.* **1987**, *40*, 247.
(72) Madden, P. A.; O'Sullivan, K.; Board, J. A.; Fowler, P. W. *J. Chem. Phys.* **1991**, *94*, 918.
(73) Kirillov, S. A.; Yannopoulos, S. N. *Phys. Rev. B* **2000**, *61*, 11391.
(74) Ribeiro, M. C. C.; Wilson, M.; Madden, P. A. *J. Chem. Phys.* **1999**, *110*, 4803.
(75) Castiglione, M. J.; Ribeiro, M. C. C.; Wilson, M.; Madden, P. A. *Z. Naturforsch.* **1999**, *54a*, 605.
(76) Akdeniz, Z.; Madden, P. A. *J. Phys. Chem. B* **2006**, *110*, 6683.
(77) Angell, C. A. *Science* **1995**, *267*, 1924.
(78) Kivelson, D.; Tarjus, G. *J. Non-Cryst. Solids* **1998**, *235−237*, 86.
(79) Angell, C. A. *J. Phys.: Condens. Matter* **2000**, *12*, 6463.
(80) Xu, W.; Cooper, E. I.; Angell, C. A. *J. Phys. Chem. B* **2003**, *107*, 6170.
(81) Ingram, J. A.; Moog, R. S.; Ito, N.; Biswas, R.; Maroncelli, M. *J. Phys. Chem. B* **2003**, *107*, 5926.
(82) Ito, N.; Arzhantsev, S.; Maroncelli, M. *Chem. Phys. Lett.* **2004**, *83*, 396.
(83) Johari, G. P. *J. Chem. Phys.* **2000**, *112*, 10957.
(84) Kauzmann, W. *Chem. Rev.* **1948**, *43*, 219.
(85) Wang, L. M.; Velikov, V.; Angell, C. A. *J. Chem. Phys.* **2002**, *117*, 10184.
(86) Thirumalai, D.; Mountain, R. D.; Kirkpatrick, T. R. *Phys. Rev. A* **1989**, *39*, 3563.
(87) Sillescu, H. *J. Non-Cryst. Solids* **1999**, *243*, 81.
(88) Glotzer, S. C. *J. Non-Cryst. Solids* **2000**, *274*, 342.
(89) Chelli, R.; Cardini, G.; Procacci, P.; Righini, R.; Califano, S. *J. Chem. Phys.* **2003**, *119*, 357.
(90) Aichele, M.; Gebremichael, Y.; Starr, F. W.; Baschnagel, J.; Glotzer, S. C. *J. Chem. Phys.* **2003**, *119*, 5290.
(91) Gebremichael, Y.; Vogel, M.; Bergroth, M. N. J.; Starr, F. W.; Glotzer, S. C. *J. Phys. Chem. B* **2005**, *109*, 15068.
(92) Giovambattista, N.; Buldyrev, S. V.; Stanley, H. E.; Starr, F. W. *Phys. Rev. E* **2005**, *72*, 011202.
(93) Cicerone, M. T.; Blackburn, F. R.; Ediger, M. D. *J. Chem. Phys.* **1995**, *102*, 471.